Atherosclerosis 287 (2019) 70–80

Contents lists available at ScienceDirect

Atherosclerosis

journal homepage: www.elsevier.com/locate/atherosclerosis

CD13 deficiency leads to increased oxidative stress and larger atherosclerotic lesions

Charan V. Devarakonda[a], Flavia E. Pereira[a], Jonathan D. Smith[b], Linda H. Shapiro[a,*], Mallika Ghosh[a,**]

[a] Center for Vascular Biology, University of Connecticut Health Center, Farmington, CT, 06030, USA
[b] Department of Cellular and Molecular Medicine, Lerner Research Institute, Cleveland Clinic, Cleveland, OH, 44195, USA

HIGHLIGHTS

- CD13 deficiency in bone marrow derived macrophages led to increased nitric oxide production (oxidative stress) with oxLDL treatment.
- Increased oxidative stress in CD13 deficient bone marrow derived macrophages led to amplified apoptosis.
- Absence of CD13 led to larger atherosclerotic lesions in high fat diet-fed $CD13^{-/-}Ldlr^{-/-}$ mice.
- Atherosclerotic lesions from $CD13^{-/-}Ldlr^{-/-}$ mice contained higher number of apoptotic cells.

ARTICLE INFO

Keywords:
CD13
ANPEP
Atherosclerosis
Oxidative stress
oxLDL
Macrophages
Reactive oxygen species
Reactive nitrogen species
Nitric oxide
L-NMMA
NAC

ABSTRACT

Background and aims: Atherosclerosis is an inflammatory cardiovascular disorder characterized by accumulation of lipid-loaded macrophages in the intima. Prolonged accumulation leads to apoptosis of macrophages and eventually to progression of lesion development. Prevention of macrophage accumulation within the intima has been shown to reduce lesion formation. Since CD13 mediates trafficking of macrophages to sites of injury and repair, we tested the role of CD13 in atherosclerosis.

Methods: $CD13^{+/+}Ldlr^{-/-}$ and $CD13^{-/-}Ldlr^{-/-}$ (low density lipoprotein receptor) mice were fed basal or high fat diet (HFD) for 9, 12 and 15 weeks. Mice were euthanized and aortic roots along with innominate arteries were analyzed for atherosclerotic lesions. Cellular mechanisms were determined *in vitro* using $CD13^{+/+}$ and $CD13^{-/-}$ bone marrow derived macrophages (BMDMs) incubated with highly oxidized low-density lipoprotein (oxLDL).

Results: At the 9 and 12 week time points, no differences were observed in the average lesion size, but at the 15 week time point, $CD13^{-/-}Ldlr^{-/-}$ mice had larger lesions with exaggerated necrotic areas. $CD13^{+/+}$ and $CD13^{-/-}$ macrophages endocytosed similar amounts of oxLDL, but $CD13^{-/-}$ macrophages generated higher amounts of oxidative stressors in comparison to $CD13^{+/+}$ macrophages. This increased oxidative stress was due to increased nitric oxide production in oxLDL treated $CD13^{-/-}$ macrophages. Accumulated oxidative stress subsequently led to accelerated apoptosis and enhanced necrosis of oxLDL treated $CD13^{-/-}$ macrophages.

Conclusions: Contrary to our prediction, CD13 deficiency led to larger atherosclerotic lesions with increased areas of necrosis. Mechanistically, CD13 deficiency led to increased nitric oxide production and consequently, greater oxidative stress.

1. Introduction

Atherosclerosis is an inflammatory cardiovascular disorder driven primarily by macrophages in both initiation and progression of the disease. Atherosclerotic lesion development is characterized by accumulation of lipid-loaded, functionally impaired macrophages in the

Abbreviations: BMDMs, bone marrow derived macrophages; ROS, reactive oxygen species; RNS, reactive nitrogen species; TLR4, toll-like receptor 4; NO, nitric oxide; iNOS, inducible nitric oxide synthase; L-NMMA, N^G-Monomethyl-L-arginine, monoacetate salt; NAC, *N*-Acetyl-L-cysteine

* Corresponding author. 263 Farmington Avenue, Farmington, CT, 06030, USA.
** Corresponding author. 263 Farmington Avenue, Farmington, CT, 06030, USA.
E-mail addresses: lshapiro@uchc.edu (L.H. Shapiro), mghosh@uchc.edu (M. Ghosh).

https://doi.org/10.1016/j.atherosclerosis.2019.06.901
Received 31 May 2018; Received in revised form 6 June 2019; Accepted 12 June 2019
Available online 13 June 2019

intima of large vessels [1]. Intimal lipid-loaded macrophages eventually die by apoptosis [2] and in advanced lesions, accumulate and overwhelm normal clearance mechanisms. This results in the formation of large necrotic areas that can rupture and initiate thrombus formation leading to stroke or myocardial infarction. Not surprisingly, systemic depletion of macrophages [3] or macrophage-specific deletion of inflammatory signaling mediators such as TLR4[4], MyD88[4] and IRF3 [5] has been shown to reduce atherosclerotic burden and highlights the critical role of macrophages in initial lesion development. Therefore, a better understanding of the molecules and pathways contributing to macrophage infiltration and retention in the intima will be useful in designing optimal therapeutic strategies.

CD13 is a multifunctional, cell-surface N-terminal aminopeptidase that plays an important role in pro-inflammatory processes such as TLR4 signaling [6], receptor-mediated, dynamin-dependent endocytosis of various receptors [7], angiogenesis [8], cell-cell and cell-matrix adhesion [9] and monocyte trafficking and macrophage accumulation in inflammatory sites [10]. Since these processes all play vital roles in inflammation and, consequently, initiation and progression of atherosclerotic lesions, we hypothesized that CD13 will exacerbate disease by promoting inflammation and thus intensify atherosclerotic lesion formation.

In this study, we directly addressed the role of CD13 in atherosclerosis using the *Ldlr*-deficient, high fat diet (HFD) atherosclerotic model crossed with $CD13^{+/+}$ (wild type) and $CD13^{-/-}$ mice. Contrary to our prediction, we observed that over time the lack of *CD13* resulted in larger atherosclerotic lesions characterized by an increase in lesional necrotic area and higher numbers of apoptotic cells. Determining the cellular mechanisms underlying this phenotype led us to conclude that $CD13^{-/-}$ macrophages generate higher amounts of oxidative stress due to increased nitric oxide production. We have previously shown that the absence of CD13 leads to increased nitric oxide production with LPS treatment due to biased endosomal TLR4 signaling [6]. In this study, we show that the increased nitric oxide production is also seen in the context of oxLDL treatment. From these results, we also established the critical role of CD13 in maintaining homeostatic levels of oxidative stressors.

2. Materials and methods

We declare that all supporting data are available within the article and Supplemental Files.

2.1. Generation of $CD13^{-/-}Ldlr^{-/-}$ mice

Global $CD13^{-/-}$ mice (C57BL/6J strain) generated in our lab [11] were crossed to $Ldlr^{-/-}$ mice to generate $CD13^{+/-}Ldlr^{+/-}$ heterozygote mice. Heterozygote mice were crossed to generate $CD13^{-/-}Ldlr^{-/-}$ mice. Tail snips were genotyped to identify double knockout mice and immunoblots for CD13 and Ldlr were performed to validate knockout of *CD13* and *Ldlr*. Parental $Ldlr^{-/-}$ mice were used as *CD13* wild type controls. Female $CD13^{+/+}Ldlr^{-/-}$ and $CD13^{-/-}Ldlr^{-/-}$ mice were saved for breeding and only male mice were used for all *in vivo* experiments. Mice were housed in animal facilities at University of Connecticut Health Center and all experiments were performed in accordance with a protocol approved by The Institutional Animal Care and Use Committee.

2.2. High fat diet (HFD)

High fat diet (TD.88137) was purchased from Harlan Teklad and is currently available from Envigo, IN, USA. Mice were fed basal diet or HFD for 9, 12 and 15 weeks.

2.3. Total cholesterol and triglycerides quantification assay

Plasma from basal diet and high fat diet fed mice was collected and total cholesterol as well as triglycerides content was determined using Cholesterol LiquiColor kit (1010) and LiquiColor Triglycerides kit (2100) (Stanbio, TX, USA), respectively. Cholesterol standards ranging from 0 to 200 mg/dL and plasma samples were mixed with cholesterol reagent and incubated for 20 min at 37 °C. Triglyceride standards ranging from 0 to 200 mg/dL and plasma samples were mixed with triglyceride activated reagent and incubated for 10 min at 37 °C. Absorbance was read at 500 nm, cholesterol and triglyceride content was determined using respective standards.

2.4. Immunofluorescence analysis

Frozen sections of innominate arteries were hydrated in PBS and blocked with 1% BSA/PBS. Sections were incubated with primary antibodies for 2 h at room temperature. Primary antibodies were detected with fluorophore conjugated secondary antibodies and nuclei were stained with DAPI.

Fluorescent images were analyzed with Fiji software [12] to determine the percentage of positively stained cells. Individual channel images were converted to 8-bit and regions of interest were drawn to encapsulate the plaques. Threshold levels for each channel were determined and kept constant between different images. Size tool was used to identify intact cells and total number of cells were determined using analyze particles tool. Number of positively stained cells were normalized to total number of cells (DAPI positive) and expressed as a percentage.

2.5. TUNEL assay and efferocytosis analysis

Click-iT™ Plus TUNEL assay kit was purchased from Thermo Fisher scientific, MA, USA (C10618). Formalin fixed paraffin embedded sections of aortic roots were stained as per manufacturer's instructions. Sections were subsequently immunostained with F4/80 antibody to identify macrophages. Fluorescent images were taken from multiple regions within the lesions. Total number of apoptotic cells were determined by counting the number of TUNEL positive cells. For efferocytosis analysis, TUNEL positive cells were classified as either “macrophage associated” if they were found within or closely associated with F4/80 positive cells or “free” if they were not within or closely associated with F4/80 positive cells. Efferocytosis efficiency was determined by calculating the ratio of free to macrophage-associated apoptotic cells with a high ratio indicating reduced efferocytosis.

2.6. Histochemical analysis of atherosclerotic lesions

2.6.1. Oil red O staining

Frozen sections of aortic roots were fixed with 4% PFA and stained with Oil red O (C.I. 26125, Sigma-Aldrich, MO, USA) for 15 min at room temperature. Sections were counterstained with hematoxylin QS for 40 s. Slides were mounted with glycerol/PBS and bright field images were taken. Images were analyzed with Image-Pro Plus software to determine the density of Oil red O stain within the lesions.

2.6.2. Hematoxylin and Eosin staining

Frozen sections of innominate arteries were hydrated and stained with Hematoxylin and Eosin stain. Bright field images were analyzed with Fiji software. Necrotic area within the lesions were identified as regions devoid of cells. Necrotic area was normalized to total lesional area and expressed as percent necrotic area.

2.6.3. Trichrome staining

Masson's 2000 trichrome kit was purchased from American MasterTech Inc., CA, USA (KTMTR2). Formalin fixed paraffin

embedded sections of aortic roots were stained using microwave method as per manufacturer's instructions. Bright field images were analyzed with Fiji software to quantify the necrotic area as well as the total lesion area.

2.6.4. Bone marrow derived macrophages (BMDMs) and oxidized LDL (oxLDL)

Bone marrow cells were obtained from femur and tibia of 3 different $CD13^{+/+}$ and $CD13^{-/-}$mice for every experiment. Red blood cells were lysed, and bone marrow cells were seeded in DMEM medium supplemented with 10% fetal bovine serum, penicillin, streptomycin and 20 ng/mL M-CSF (315-02, Peprotech, NJ, USA). Fresh media was added on day 3 and cells were cultured for 5 days in differentiation media. All experiments on BMDMs were started on day 5.

Different lots of oxLDL (J65261 - Alfa Aesar, MA, USA) were used for all experiments and the oxLDL content ranged from 35.7 to 86 nmoles of MDA/mg of protein. The majority of the experiments were performed with 80 μg/mL of oxLDL with only the apoptosis assay being performed with both 80 μg/mL and 150 μg/mL of oxLDL.

2.6.5. Isolation of cells from aorta for flow cytometry analysis

Mice were sedated with ketamine-xylazine and perfused with cold PBS supplemented with 20 U/mL Heparin at a speed of 2 mL/min for a total of 20 min. Aortas were harvested from the root of the aortic arch until the abdominal iliac bifurcation and all the fat was removed. Washed aortas were digested with 1 mL of pre-warmed digestion buffer (2% FBS, 0.05% w/v hyaluronidase, 0.3% w/v collagenase and PBS). Tissue was minced and digested for a total of 3 times with 10 min for the first 2 digestions and 15 min for the third digestion at 37 °C. After each digestion, tissue was pipetted vigorously (20–25 times) and supernatant was collected in a fresh tube containing 3–5 mL of FACS buffer. Collagenase was removed by spinning the cells at 1200 rpm for 5 min at 4 °C and suspended the cells in fresh FACS buffer. After collecting all the fractions, cells were filtered through 40 μm filter, counted and stained with appropriate antibodies for flow cytometry.

2.6.6. FITC annexin V apoptosis analysis

Untreated and oxLDL treated BMDMs were detached using cold PBS supplemented with 2% FBS and 2 mM EDTA. 0.1×10^6 cells were mixed with 5 μL each of FITC Annexin V and PI (556547 - BD Biosciences, CA, USA). Stained cells were analyzed by flow cytometry with appropriate controls. Late apoptotic cells were identified as FITC Annexin V and PI double positive cells. The net increase in apoptosis due specifically to oxLDL treatment was assessed by subtracting basal apoptotic rates from their respective oxLDL treated levels.

2.6.7. Dil-oxLDL uptake assay

BMDMs were left untreated or treated with Dil-oxLDL (J64164 - Alfa Aesar, MA, USA) alone or Dil-oxLDL and dynasore for 3 h, 6 h and 24 h. At the end of different time points, BMDMs were lysed with RIPA lysis buffer and total protein content was determined. Fluorescence intensity of Dil-oxLDL was determined using an excitation wavelength of 520 nm and read at an emission wavelength of 590 nm. Dil-oxLDL amounts were determined using standards (0–1000 ng) in RIPA lysis buffer and normalized to total protein content.

2.6.8. In vitro detection of reactive oxygen species (ROS) and reactive nitrogen species (RNS)

ROS and RNS were detected using H2DCFDA dye (Thermo Fisher scientific, D399). BMDMs in 96-well plates were pre-loaded with H2DCFDA dye (50 μM) for 50 min at 37 °C. Cells were left untreated or treated with oxLDL alone or oxLDL and dynasore (40 μM) in phenol red free media for 2 h30 min at 37 °C. Hoechst was added to all the wells and incubated for an additional 30 min at 37 °C. Fluorescence intensity of DCF was determined using an excitation wavelength of 485 nm and read at an emission wavelength of 530 nm. Fluorescence intensity of Hoechst was determined using an excitation wavelength of 340 nm and read at an emission wavelength of 480 nm. Fluorescence intensity of DCF was normalized to fluorescence intensity of Hoechst from the same well.

2.6.9. L-NMMA (N^G-Monomethyl-L-arginine, monoacetate salt) and NAC (N-acetyl-L-cysteine) treatment

L-NMMA (ab120137 – Abcam, MA, USA) and NAC (A9165 - Sigma-Aldrich, MO, USA) were obtained. BMDMs in 96-well plates were pre-loaded with H2DCFDA dye (50 μM) for 50 min at 37 °C. Cells were left untreated or treated with oxLDL alone or oxLDL + NMMA (0.5 mM) or oxLDL + NAC (10 mM) in phenol red free media for 1 h at 37 °C. Proceeded with measurement and normalization of DCF fluorescence intensity as mentioned above.

2.6.10. Nitric oxide assay

Fluorometric nitric oxide assay kit (ab65327 – Abcam, MA, USA) was obtained. BMDMs were left untreated or treated with oxLDL for 1 h at 37 °C. Cells were collected and proceeded with nitric oxide quantification as per manufacturer's instructions.

2.6.11. MitoSOX assay

MitoSOX red mitochondrial superoxide indicator (M36008 – Thermo Fisher scientific, MA, USA) was obtained. BMDMs in 96-well plates were pre-loaded with mitoSOX (5 μM) for 1 h at 37 °C. BMDMs were left untreated or treated with oxLDL alone or oxLDL + NMMA (0.5 mM) or oxLDL + NAC (10 mM) in phenol red free media for 3 h at 37 °C. Hoechst was added to all the wells and incubated for an additional 30 min at 37 °C. Fluorescence intensity of mitoSOX was determined using an excitation wavelength of 510 nm and read at an emission wavelength of 580 nm. Fluorescence intensity of mitoSOX was normalized to fluorescence intensity of Hoechst from the same well.

2.6.12. Statistical analyses

Data from individual experiments is represented as mean ± SEM. GraphPad Prism was used to perform statistical analyses. Values from individual experiments were analyzed by Kolmogorov-Smirnov test to determine if the values were normally distributed. Values that were normally distributed were subsequently analyzed using 2-tailed Student's *t*-test and significance was determined ($*p \leq 0.05$, $**p \leq 0.01$, $***p \leq 0.001$). Values from 15 week HFD total cholesterol assay, 15 week HFD percent necrotic area and 15 week HFD necrotic area measurements were not normally distributed and hence were analyzed using non-parametric Mann-Whitney *U* test and significance was determined ($*p \leq 0.05$, $**p \leq 0.01$, $***p \leq 0.001$). All the *p* values from both Kolmogorov-Smirnov and Mann-Whitney U tests have been tabulated in the supplementary excel document.

3. Results

3.1. $CD13^{-/-}Ldlr^{-/-}$ mice developed larger atherosclerotic lesions

To determine the role of CD13 in atherosclerosis, $CD13^{+/+}Ldlr^{-/-}$ and $CD13^{-/-}Ldlr^{-/-}$ mice were fed basal or HFD and harvested after 9, 12 and 15 weeks of diet. HFD increased plasma total cholesterol (average ~1000 mg/dL) and triglyceride levels (average ~400 mg/dL) at all time points when compared to those on basal diet (average cholesterol ~155 mg/dL and average triglyceride ~100 mg/dL, Supplemental Fig. I, Fig. 1A and B). Importantly, plasma cholesterol and triglyceride levels were comparable between $CD13^{+/+}Ldlr^{-/-}$ and $CD13^{-/-}Ldlr^{-/-}$ mice fed HFD, suggesting that the lack of *CD13* did not affect metabolic processes and any observed phenotypic alterations will be independent of lipid metabolism.

Examination of individual aortic root sections harvested at various time points showed that as expected, mice fed with HFD progressively developed lesions of increasing size (as assessed by area of Oil red O

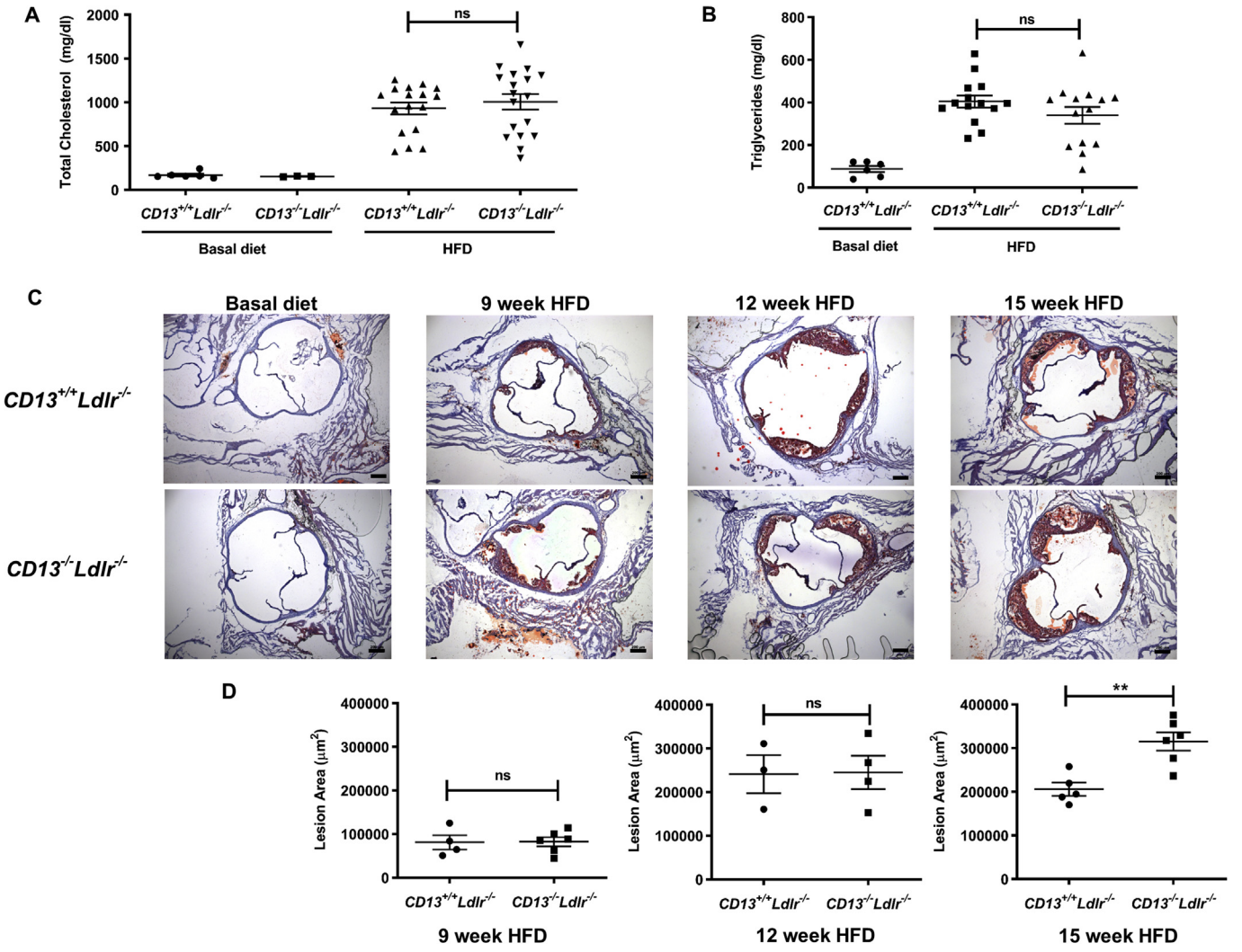

Fig. 1. *CD13*$^{-/-}$*Ldlr*$^{-/-}$ mice developed larger atherosclerotic lesions.
Levels of total fasting (4 h) plasma cholesterol (A) (n = 6, 3, 17 and 18 respectively) and triglycerides (B) (n = 6, 14 and 14 respectively) were measured in *CD13*$^{+/+}$*Ldlr*$^{-/-}$ and *CD13*$^{-/-}$*Ldlr*$^{-/-}$ mice fed basal diet or HFD for 15 weeks. Data is represented as mean ± SEM. Statistical analysis for total cholesterol assay was performed using 2-tailed Mann Whitney test while Student's *t*-test was performed on triglyceride assay values, ns (not significant). (C) Representative images of Oil red O stained aortic root sections from basal and HFD fed mice at 9 (n = 4 and 6 respectively), 12 (n = 3 and 4 respectively) and 15 week time points (n = 5 and 6 respectively). Scale bar represents 200 μm. (D) Quantification of lesion areas using Image-pro Plus software. Data is represented as mean ± SEM. Statistical analysis was performed using 2-tailed Student's *t*-test with $^{**}p < 0.01$. ns (not significant). (For interpretation of the references to colour in this figure legend, the reader is referred to the Web version of this article.)

stain), while mice on a basal diet did not acquire any lesions (Fig. 1C). Total lesion area measurements showed no differences between *CD13*$^{+/+}$*Ldlr*$^{-/-}$ and *CD13*$^{-/-}$*Ldlr*$^{-/-}$ mice (Fig. 1D) at the early time points of 9 and 12 weeks, suggesting that the formation and initial progression of lesions was unaffected by the absence of *CD13*. However, contrary to our predictions, *CD13*$^{-/-}$*Ldlr*$^{-/-}$ mice displayed larger lesions at the later time point (~1.5 fold larger, 15 weeks), indicating that the long-term progression of lesions is accelerated in *CD13*$^{-/-}$*Ldlr*$^{-/-}$ mice. Subsequent experiments were aimed at determining the potential mechanisms underlying these unexpected results.

3.2. Infiltrating immune cell profiles were identical between *CD13*$^{+/+}$*Ldlr*$^{-/-}$ and *CD13*$^{-/-}$*Ldlr*$^{-/-}$ atherosclerotic lesions

CD13 plays an important role in monocyte trafficking to and macrophage accumulation at sites of injury and repair [9,10,13] which are essential for lesion progression, prompting our initial focus on potential effects on the immune cell profile of *CD13*$^{+/+}$ and *CD13*$^{-/-}$ lesions. We restricted this analysis to the 15-week time point since the differences in lesion area were only observed at this time point (Fig. 1D). Aortas from *CD13*$^{+/+}$*Ldlr*$^{-/-}$ and *CD13*$^{-/-}$*Ldlr*$^{-/-}$ HFD fed mice were harvested individually and single cell suspensions were stained to identify different immune cell types by flow cytometry. Percentages of hematopoietic cells, macrophages, dendritic cells (Fig. 2A), T cells and B cells (Supplemental Fig. IIA and IIB) were essentially identical between the genotypes. Assessment of potential differences in macrophage (F4/80+) and dendritic cell (CD11c+) distribution in frozen sections of innominate arteries demonstrated that these populations were predominantly localized to the intima, while a small population of macrophages was present on the adventitial side (Fig. 2B). In the intima, small subsets of single-positive cells were observed, while a majority of the cells consisted of a F4/80-CD11c double-positive subset of dendritic cells [14] (Fig. 2B). To enumerate the number of F4/80 and CD11c positive cells, images were quantified using Fiji software [12]. Similar to results seen with the flow analysis, no differences were observed in the percentage of F4/80 and CD11c positive cells between *CD13*$^{+/+}$*Ldlr*$^{-/-}$ and *CD13*$^{-/-}$*Ldlr*$^{-/-}$ mice on HFD (Fig. 2C). Finally, staining for Mac-3+ macrophages confirmed

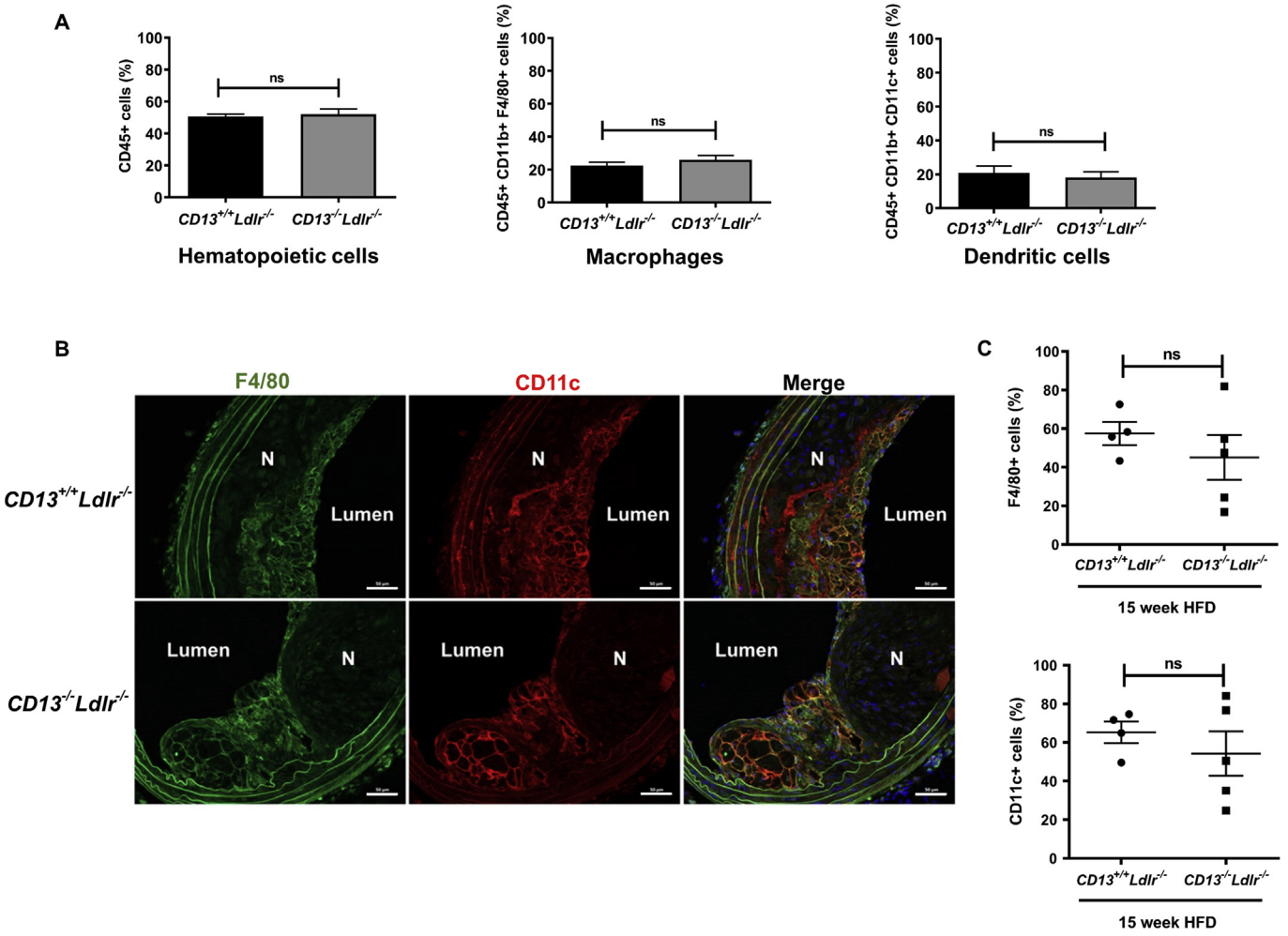

Fig. 2. Immune cell profile of $CD13^{+/+}Ldlr^{-/-}$ and $CD13^{-/-}Ldlr^{-/-}$ lesions.
(A) Flow cytometric analysis of cells derived from aortas of 15 week HFD fed $CD13^{+/+}Ldlr^{-/-}$ (n = 4) and $CD13^{-/-}Ldlr^{-/-}$ (n = 7) mice. (B) Representative fluorescent images of innominate arteries from 15 week HFD fed mice stained with F4/80 (green), CD11c (red) antibodies and DAPI (blue). Scale bar represents 50 μm, (N, Necrotic area). (C) Quantification of fluorescent images, $CD13^{+/+}Ldlr^{-/-}$ (n = 4) and $CD13^{-/-}Ldlr^{-/-}$ (n = 5) using Fiji software. Data is represented as mean ± SEM. Statistical analysis was performed using 2-tailed Student's *t*-test, (ns – not significant). (For interpretation of the references to colour in this figure legend, the reader is referred to the Web version of this article.)

these findings (Supplemental Fig. IIC and IID). These results are somewhat surprising but are consistent with our previous observations demonstrating that CD13 differentially regulates inflammatory processes depending on the site and type of inflammatory stimulus [6,10,13,15].

3.3. $CD13^{-/-}Ldlr^{-/-}$ atherosclerotic lesions showed increased necrosis and apoptosis

Infiltrating immune cell profiles were similar in $CD13^{+/+}Ldlr^{-/-}$ and $CD13^{-/-}Ldlr^{-/-}$ mice, yet the lesions were larger in mice lacking *CD13*. To understand the reasons for this disparity, we stained innominate artery sections with Hematoxylin and Eosin to compare necrotic areas within the lesions. We observed a nearly two-fold increase in normalized acellular necrotic area within the $CD13^{-/-}Ldlr^{-/-}$ lesions (~28% necrotic; Fig. 3A and B) as compared to $CD13^{+/+}Ldlr^{-/-}$ lesions (~14% necrotic; Fig. 3A and B). While this difference was not statistically significant ($p = 0.1143$), it may allude to the role of *CD13* in determining lesion characteristics. Additionally, trichrome stained aortic root sections revealed an identical increase in necrotic area in $CD13^{-/-}Ldlr^{-/-}$ lesions (Fig. 3C) as seen with innominate arteries, suggesting that the increased necrosis in the absence of CD13 is independent of the lesion location.

Necrotic cores in atherosclerotic lesions result from inadequate removal of apoptotic foam cells [16]. To determine if the increase in necrotic area in $CD13^{-/-}Ldlr^{-/-}$ lesions was due to increased apoptosis, aortic roots were analyzed using TUNEL assay to identify and enumerate apoptotic cells. Additionally, aortic roots were also incubated with F4/80 antibodies to identify macrophages within the lesions. Apoptotic cells were observed in both $CD13^{+/+}Ldlr^{-/-}$ and $CD13^{-/-}Ldlr^{-/-}$ lesions and were predominantly F4/80 positive macrophages (Fig. 3D). Quantitation of the entire lesion illustrated that at the 15 week time point $CD13^{-/-}Ldlr^{-/-}$ lesions contained a higher number of apoptotic cells (125.37 cells) in comparison to $CD13^{+/+}Ldlr^{-/-}$ lesions (37.4 cells; $p = 0.0547$), while the number of apoptotic cells were similar at the 9 and 12 week time points (Fig. 3E). This suggests that the progression of $CD13^{-/-}Ldlr^{-/-}$ lesions diverged from $CD13^{+/+}Ldlr^{-/-}$ lesions over time, resulting in increased apoptosis and lesional necrosis. In addition to increased apoptosis, inefficient efferocytosis leads to expansion of necrotic cores in advanced lesions [16]. We therefore analyzed the aortic lesions to determine if the $CD13^{-/-}Ldlr^{-/-}$ mice showed defective efferocytosis by calculating the ratio of free to macrophage-associated apoptotic cells. Similar to the increased apoptosis observed in $CD13^{-/-}Ldlr^{-/-}$ lesions at the 15-week time point, we observed decreases in efferocytosis in $CD13^{-/-}Ldlr^{-/-}$ lesions (Fig. 3F). While levels of efferocytosis in the $CD13^{+/}$

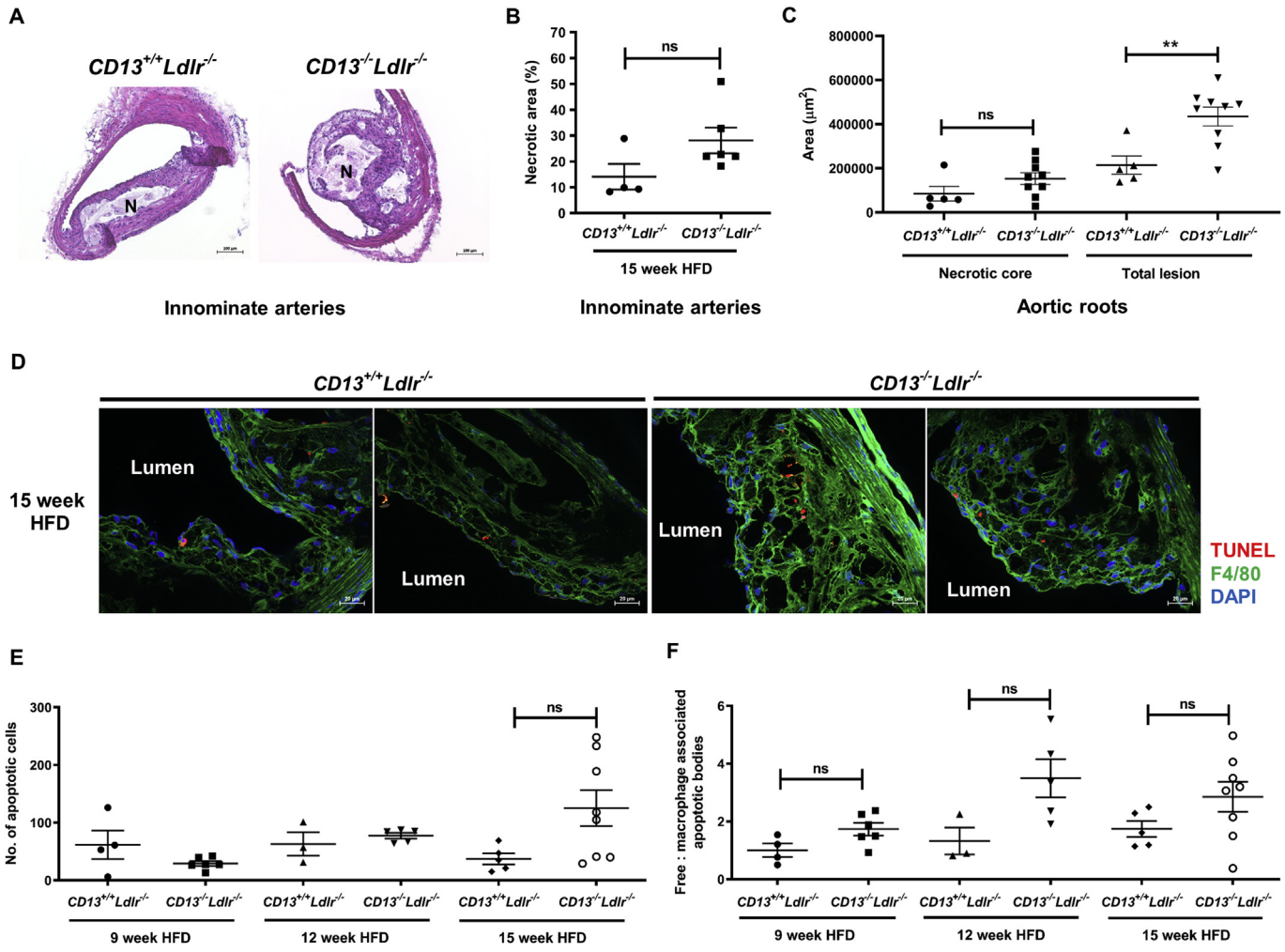

Fig. 3. *CD13*$^{-/-}$*Ldlr*$^{-/-}$ lesions contained larger necrotic areas and higher number of apoptotic cells.
(A) Hematoxylin and Eosin staining of innominate arteries from 15 week HFD fed mice. Scale bar represents 100 μm, N (necrotic area). (B) Quantification of Hematoxylin and Eosin stained bright field images using Fiji software (n = 4 and 6 respectively). Data is represented as mean ± SEM. Statistical analysis was performed using 2-tailed Mann Whitney test. (C) Quantification of trichrome stained aortic root images (15 week HFD) using Fiji software (n = 5 and 9 respectively). Data is represented as mean ± SEM. Statistical analysis was performed using Mann-Whitney test (necrotic core area) and 2-tailed Student's *t*-test (total lesion area). (D) Representative fluorescent images of aortic roots from 15 week HFD fed mice stained with TUNEL stain (red), F4/80 (green) and DAPI (blue). Scale bar represents 20 μm. (E and F) Quantification of TUNEL stained images using Fiji software to determine total number of apoptotic cells (E) and efferocytosis efficiency (F) (n = 4, 6, 3, 5, 5 and 8 respectively). Data is represented as mean ± SEM. Statistical analysis was performed using 2-tailed Student's *t*-test with $^{**}p < 0.01$. ns (not significant). (For interpretation of the references to colour in this figure legend, the reader is referred to the Web version of this article.)

$^{+}$*Ldlr*$^{-/-}$ lesions were similar at all 3 time points, efferocytosis progressively decreased in *CD13*$^{-/-}$*Ldlr*$^{-/-}$ lesions over time. While the variability of the data precluded statistical significance, clearly efferocytosis of apoptotic cells is reduced in the absence of CD13 ($p = 0.0589$, $p = 0.0607$, $p = 0.1407$ for 9, 12 and 15 week time points). Taken together, the absence of CD13 led to increased apoptosis as well as reduced efferocytosis, which together result in larger necrotic areas seen in the *CD13*$^{-/-}$*Ldlr*$^{-/-}$ lesions.

3.4. OxLDL treatment induced significantly higher apoptosis in *CD13*$^{-/-}$ BMDMs

High fat diet increases the concentration of circulating lipids, particularly oxidized LDL (oxLDL) [17], that are internalized by macrophages via receptor-mediated endocytosis, promoting foam cell formation [18] and eventual apoptotic cell death [19,20]. Initially, to determine if the differential rates of apoptotic cell death were due to lipid-mediated mechanisms, we incubated *CD13*$^{+/+}$ and *CD13*$^{-/-}$ BMDMs with highly oxidized LDL for 24 h to mimic the high lipid environment [17]. We chose to analyze apoptotic cells by flow cytometric analysis of Annexin V-FITC and PI stained cells to closely monitor the progression of apoptosis from early (annexin +/PI -) to late/end stage apoptosis (annexin +/PI +) to necrotic cells (annexin -/PI +) [21]. OxLDL treatment of BMDMs of both genotypes increased the percentage of double-positive, late-apoptotic cells over basal readings. However, apoptosis in BMDMs lacking *CD13* was surprisingly and consistently higher than *CD13*$^{+/+}$ macrophages. Specifically, untreated *CD13*$^{-/-}$ macrophages averaged 25.83% apoptotic cells as compared to 9.97% in *CD13*$^{+/+}$ macrophages (Fig. 4A and B). Analogously, oxLDL treatment of *CD13*$^{+/+}$ BMDMs showed an increase in the percentage of apoptotic cells from 9.97% to 22.06%, while *CD13*$^{-/-}$ BMDMs rose from 25.83% to 47.73% (Fig. 4B), resulting in a nearly two-fold net increase in the rate of oxLDL-induced apoptosis in *CD13*$^{-/-}$ macrophages (*CD13*$^{+/+}$ = 12.09% vs. *CD13*$^{-/-}$ = 21.9%, Fig. 4C).

To further investigate the mechanisms underlying the increased apoptosis in *CD13*$^{-/-}$ BMDMs, we treated *CD13*$^{+/+}$ and *CD13*$^{-/-}$ BMDMs with two different concentrations of oxLDL (80 μg/mL and 150 μg/mL) and monitored their progression through the different stages of apoptosis over time (24 h and 48 h post-oxLDL treatment). As previously, cells were classified as early apoptotic (annexin +/PI -),

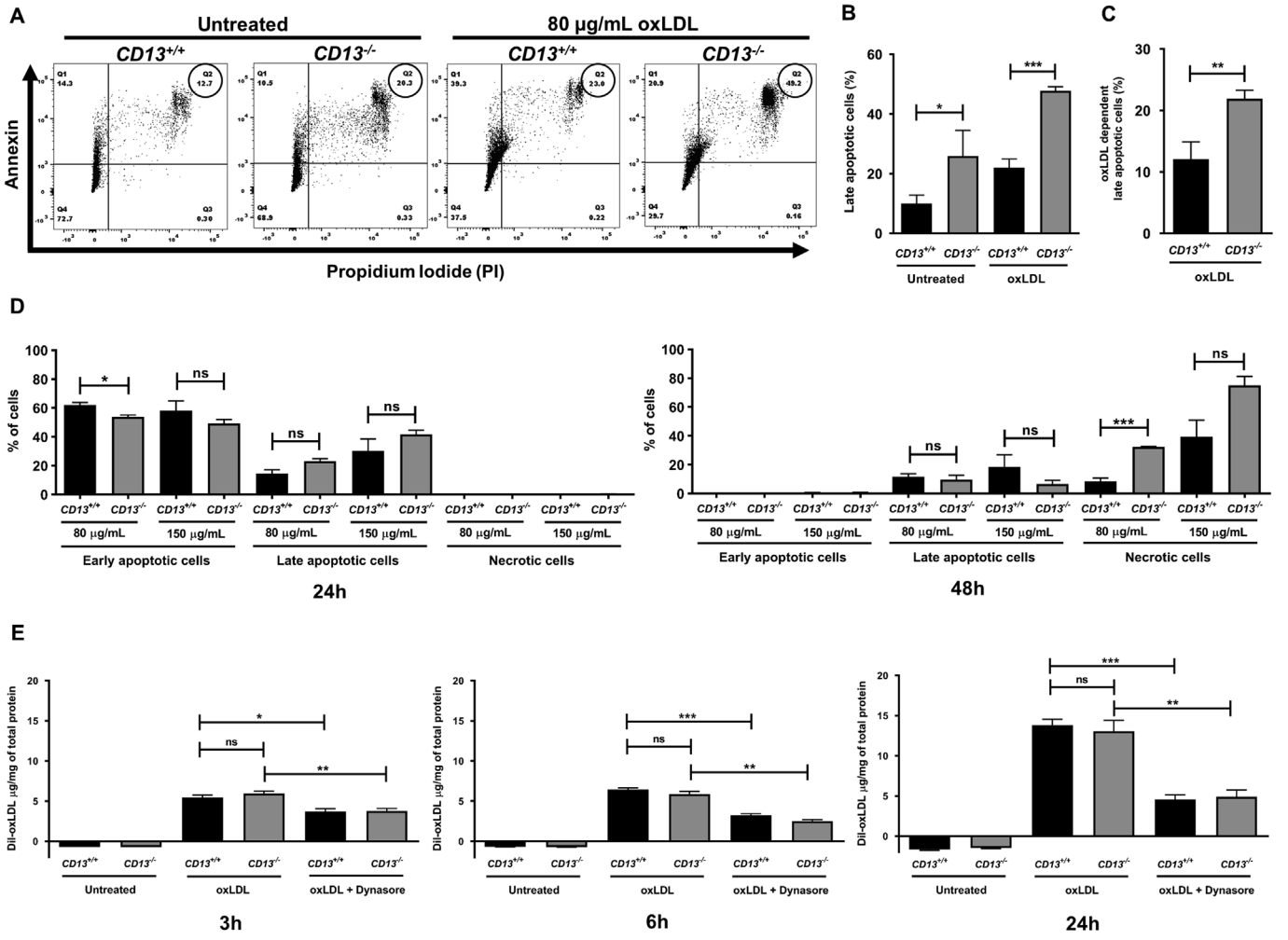

Fig. 4. OxLDL induced significantly amplified apoptosis in *CD13*$^{-/-}$ BMDMs.
(A) Representative flow histograms of untreated and oxLDL (80 µg/mL) treated BMDMs stained with Annexin V FITC and propidium iodide (PI). Apoptotic cells were classified as Annexin and PI double positive cells. (B) Quantification of percent apoptotic cells from flow histograms (n = 3 per genotype). (C) Quantification of percent apoptotic cells due specifically to oxLDL treatment (oxLDL minus untreated) (n = 3 per genotype). (D) Quantification of early apoptotic, late apoptotic and necrotic *CD13*$^{+/+}$ and *CD13*$^{-/-}$ BMDMs treated with either 80 µg/mL or 150 µg/mL oxLDL and analyzed after 24 h and 48 h by flow cytometry (n = 3 per genotype). (E) Dil-oxLDL uptake assay - *CD13*$^{+/+}$ and *CD13*$^{-/-}$ BMDMs (n = 3 per genotype) were incubated with Dil-oxLDL (20 µg/mL) for 3 h, 6 h and 24 h respectively. Uptake was determined by quantifying fluorescence intensity of extracted Dil-oxLDL and normalized to total protein content. Data is represented as mean ± SEM. Statistical analysis was performed using 2-tailed Student's *t*-test, $*p \leq 0.05$, $**p \leq 0.01$, $***p \leq 0.001$.

late or end stage apoptotic (annexin +/PI +) and necrotic cells (annexin -/PI +). Flow cytometric analysis at the 24 h time point indicated that the percentage of early apoptotic cells in *CD13*$^{+/+}$ macrophages was higher than in *CD13*$^{-/-}$ macrophages at both oxLDL doses (Supplemental Fig. III and Fig. 4D). Alternatively, this analysis clearly revealed an accelerated, dose-dependent progression of oxLDL-treated *CD13*$^{-/-}$ BMDMs to late apoptosis as compared to *CD13*$^{+/+}$ BMDMs (Supplemental Fig. III and Fig. 4D) ($p = 0.0547$ for 80 µg/mL late apoptotic cells), while necrotic cells were absent at 24 h in both genotypes in all conditions. However, by 48 h, the early apoptotic cells seen at the 24 h time point were completely absent in both genotypes (Fig. 4D), accompanied by a reduction in the percentage of late apoptotic cells. However, in contrast to the 24 h time point, necrotic cells predominated at 48 h and the *CD13*$^{-/-}$ macrophages displayed uniformly higher percentages of necrotic cells in a dose-dependent manner in comparison to *CD13*$^{+/+}$ BMDMs. Additionally, *CD13*$^{-/-}$ BMDMs showed increased levels of the apoptosis-dependent protein fragment, cleaved PARP, validating the flow findings (Supplemental Fig. IV). In summary, cells lacking CD13 showed increased apoptosis in response to oxLDL treatment.

Finally, it is formally possible that the lack of CD13 alters the *in vitro* differentiation of myeloid cells, thus potentially affecting apoptosis. However, flow analysis confirmed that untreated and oxLDL-treated BMDMs of both genotypes showed identical differentiation profiles with regard to classical myeloid differentiation markers (CD11b, F4/80, CD206, Supplemental Fig. VA and B), suggesting that the increased apoptosis in *CD13*$^{-/-}$ BMDMs was independent of the differentiation status of macrophages. Therefore, using a combination of both flow cytometric analyses of apoptosis progression and traditional protein cleavage assays, apoptosis is distinctly enhanced and accelerated in BMDMs lacking *CD13*.

OxLDL treatment and its subsequent endocytic uptake [22] have been shown to induce apoptosis of macrophages in a dose-dependent manner. We have previously shown that CD13 is a negative regulator of receptor-mediated endocytic uptake in macrophages and dendritic cells [6,7], raising the possibility that increased lipid endocytosis in the absence of CD13 underlies the increase in apoptotic cell death observed in both the *CD13*$^{-/-}$ lesions and *CD13*$^{-/-}$ BMDMs. We incubated *CD13*$^{+/+}$ or *CD13*$^{-/-}$ BMDMs with fluorescent Dil-oxLDL for 3 h (early), 6 h (intermediate) and 24 h (late) time points to assess influences of CD13 on the kinetics and degree of ligand uptake. Subsequently, cells were lysed and fluorescence intensity of internalized Dil-

oxLDL measured and normalized to total protein content. Endocytosis of Dil-oxLDL was observed at the earliest time point (3 h) and increased over time (Fig. 4E). However, no difference in uptake was seen between $CD13^{+/+}$ and $CD13^{-/-}$ BMDMs at all time points. Inhibition of dynamin-dependent endocytosis with the dynamin inhibitor dynasore significantly reduced uptake of Dil-oxLDL, but again no differences were observed between $CD13^{+/+}$ and $CD13^{-/-}$ BMDMs. This was also consistent with the patterns of expression of cell surface receptors for oxLDL between $CD13^{+/+}$ and $CD13^{-/-}$ BMDMs. Flow analysis of CD36 (major oxLDL receptor) [18] and Lox-1 [23] revealed that the percentage of CD36 and Lox-1 positive cells in untreated BMDMs was identical (Supplemental Fig. VIA and VIB). Also, oxLDL treatment led to internalization of CD36 and Lox-1 receptors to similar extent in both $CD13^{+/+}$ and $CD13^{-/-}$ BMDMs (Supplemental Fig. VIA and VIB). From these results, it is clear that CD13 does not regulate endocytosis of oxLDL and the increase in apoptosis was likely due to differences in post-uptake processes.

3.5. OxLDL-treated $CD13^{-/-}$ BMDMs produced higher levels of oxidative stress

OxLDL uptake drives pro-inflammatory signaling [24] which stimulates ROS production [25] and subsequent oxidative stress that if unresolved, leads to apoptosis. To test the role of CD13 on cellular production of oxidative stressors, $CD13^{+/+}$ and $CD13^{-/-}$ BMDMs were pre-loaded with H2DCFDA dye (fluorescent indicator of ROS and RNS levels) [26] and treated with oxLDL or oxLDL + Dynasore. Measurement of fluorescence intensity of DCF dye (oxidatively-activated) after 3 h indicated that while oxidative stress increased upon oxLDL treatment in both $CD13^{+/+}$ and $CD13^{-/-}$ BMDMs, the levels were significantly higher in $CD13^{-/-}$ BMDMs (Fig. 5A and B). This increase was mediated by dynamin-dependent oxLDL endocytosis, since inhibition of uptake by dynasore abolished the production of oxidative stressors in both $CD13^{+/+}$ and $CD13^{-/-}$ BMDMs to similar levels. Combining these results with the uptake analysis, it is evident that $CD13^{-/-}$ BMDMs endocytose similar amounts of oxLDL in comparison to $CD13^{+/+}$ BMDMs and yet show increased oxidative stress.

The important role played by TLR4 (Toll-like receptor 4) in oxLDL uptake and subsequent signaling has been well established [4,27,28]. The absence of TLR4 or MyD88 has been shown to reduce the atherosclerotic burden as well as plaque infiltration of macrophages [4]. We have previously shown that the LPS-TLR4 signaling in cells lacking CD13 is biased towards endosomal signaling pathways, leading to increased iNOS (inducible nitric oxide synthase) production and subsequently augmented nitric oxide levels [6]. We therefore hypothesized that the oxLDL treatment of $CD13^{-/-}$ BMDMs could lead to increased nitric oxide production. To this end, $CD13^{+/+}$ and $CD13^{-/-}$ BMDMs were treated short-term (1 h) with oxLDL, lysed and total nitric oxide content normalized to total protein levels. In agreement with our previous observations with LPS treatment, oxLDL treatment of $CD13^{-/-}$ BMDMs resulted in higher amounts of nitric oxide in comparison to $CD13^{+/+}$ BMDMs (21.1 pmol/μg vs 10.8 pmol/μg, respectively Fig. 5C). In addition, untreated $CD13^{-/-}$ BMDMs also generated higher amounts of nitric oxide compared to untreated wild type controls (12.1 pmol/μg vs 6.96 pmol/μg), suggesting a basal dysregulation of nitric oxide production in the absence of CD13. To confirm the oxLDL-dependent increase in iNOS production, we treated $CD13^{+/+}$ and $CD13^{-/-}$ BMDMs with oxLDL and an iNOS inhibitor, L-NMMA (N^G-Monomethyl-L-arginine, monoacetate salt) and performed H2DCFDA analysis as before. As predicted, the treatment of $CD13^{-/-}$ BMDMs with oxLDL and L-NMMA reduced the levels of RNS and eliminated the difference between the genotypes (Fig. 5D). Importantly, inhibition of iNOS did not eliminate total oxidative stressors in either genotype, since L-NMMA treatment did not reduce DCF fluorescence intensity to that of untreated cells. Alternatively, treatment with the pan-antioxidant NAC (*N*-Acetyl-L-cysteine) resulted in overall DCF fluorescence intensity similar to untreated samples (Fig. 5D), suggesting that while nitric oxide is a major oxidative stressor produced upon oxLDL treatment, other species are clearly induced as well.

The role of mitochondrial oxidative stress in atherosclerosis has generated significant interest with studies showing that the alleviation of mitochondrial oxidative stress reduces atherosclerosis [29–31]. To investigate potential contributions of CD13 to mitochondrial stress, we measured the levels of mitochondrial reactive oxygen species using mitoSOX, a fluorogenic dye that specifically reacts with mitochondrial superoxide to generate a fluorescent product [32]. Similar to the total cellular oxidative stressor levels, oxLDL treated $CD13^{-/-}$ BMDMs generated higher amounts of mitochondrial superoxide compared to $CD13^{+/+}$ BMDMs (Fig. 5E) ($p = 0.0529$, $p = 0.1826$, $p = 0.4950$ for oxLDL, oxLDL + NMMA and oxLDL + NAC treatments, respectively). However, the increase in mitochondrial superoxide levels in $CD13^{-/-}$ BMDMs was much lower in magnitude compared to the increase in the total cellular oxidative stressor levels, suggesting a limited contribution from the mitochondria and that the predominant oxidative stressor produced in oxLDL-treated $CD13^{-/-}$ BMDMs is cytosolic nitric oxide. This notion is further validated by the inability of the inhibitors NMMA and NAC to reduce mitochondrial oxidative stress to the levels of untreated BMDMs (Fig. 5E).

In summary, using the HFD, $Ldlr^{-/-}$ model of atherosclerosis we have shown *in vivo* that the absence of CD13 generates larger atherosclerotic lesions accompanied by increased lesional cell apoptosis and overall necrosis. Mechanistically, we demonstrate that *in vitro,* BMDMs lacking CD13 show increased levels of oxidative stress in response to oxLDL uptake and, consistent with our *in vivo* phenotype, ultimately amplify cell death by apoptosis.

4. Discussion

While we have previously shown that CD13 mediates endothelial/monocyte adhesion in inflammatory processes [9], the immune and vascular systems of unchallenged $CD13^{-/-}$ mice are physiologically normal with standard hematopoietic profiles and myeloid cell functions [11]. However, in various sterile injury models, we found that the lack of CD13 leads to distinct cellular and physiological responses that depend on the type of challenge and tissue involved. For instance, $CD13^{-/-}$ mice subjected to myocardial infarction via coronary artery occlusion [10] or thioglycollate-induced peritonitis [33] showed dramatic reductions in the number of infiltrating immune cells and compromised infarct healing [10,13]. On the other hand, peripheral artery occlusion in $CD13^{-/-}$ mice reduced infiltration of only the pro-inflammatory dendritic cell subset (DCs) while other immune cell populations were equivalent to wild type ischemic muscle [15]. While this DC-low phenotype logically would be considered pro-healing, repair of the muscle tissue in these mice was impaired [15], clearly indicating that the profile of migrating immune cells has specific and context-dependent physiological effects, presumably dependent on the nature of injury and infiltrating cells as well as on the microenvironmental conditions.

Based on this knowledge, we assessed the contribution of CD13 in atherosclerosis, a cardiovascular disorder driven by chronic and aberrant inflammatory responses, hypothesizing that the lack of CD13 would be atheroprotective. Contrary to our belief, $CD13^{+/+}Ldlr^{-/-}$ and $CD13^{-/-}Ldlr^{-/-}$ mice on HFD showed equivalent numbers of infiltrating immune cells in atherosclerotic lesions, indicating that the initial recruitment and entrapment of macrophages was unaffected by the absence of CD13 and supports the notion that the number/phenotype of infiltrating immune cells is only one factor in determining atherosclerotic burden.

Atherosclerotic lesions arise from arterial endothelial damage, leading to oxLDL accumulation and monocyte infiltration from the circulation, followed by subsequent uptake of oxLDL particles by macrophages differentiated in situ [34]. Lipid-loaded macrophages are trapped in the intima [35] and eventually undergo apoptosis. In

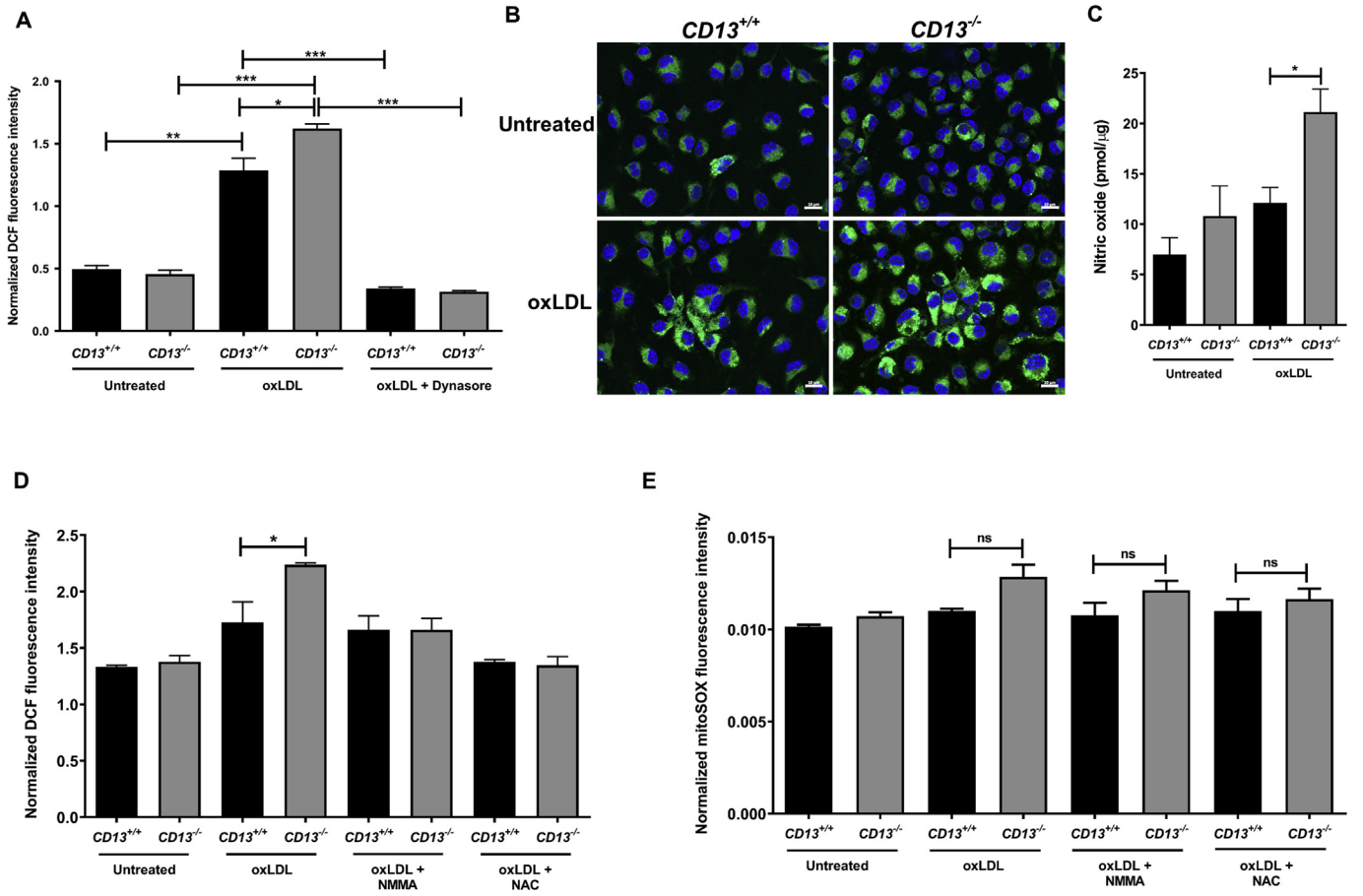

Fig. 5. *CD13*$^{-/-}$ BMDMs showed increased levels of oxidative stress in response to oxLDL treatment.
(A) Detection of oxidative stressors using H2DCFDA dye. *CD13*$^{+/+}$ and *CD13*$^{-/-}$ BMDMs (n = 3 per genotype) preloaded with H2DCFDA dye were left untreated or incubated with oxLDL (80 μg/mL) or oxLDL + dynasore for 3 h. Fluorescence intensity of DCF was normalized to Hoechst fluorescence intensity. (B) Representative DCF fluorescent images of untreated and oxLDL treated BMDMs. Scale bar represents 10 μm. (C) Measurement of nitric oxide from cell lysates left untreated or treated with oxLDL (80 μg/mL) for 1 h. (D) BMDMs pre-loaded with H2DCFDA dye were left untreated or treated with oxLDL alone (80 μg/mL) or oxLDL + NMMA (0.5 mM) or oxLDL + NAC (10 mM) for 1 h. DCF fluorescence intensity was measured as before. (E) Detection of mitochondrial ROS using mitoSOX. BMDMs pre-loaded with mitoSOX (5 μM) were left untreated or treated with oxLDL alone or oxLDL + NMMA (0.5 mM) or oxLDL + NAC (10 mM) for 3 h. Fluorescence intensity of mitoSOX was normalized to fluorescence intensity of Hoechst. Data is represented as mean ± SEM. Statistical analysis was performed using 2-tailed Student's *t*-test, $*p \leq 0.05$, $**p \leq 0.01$, $***p \leq 0.001$.

advanced lesions, apoptotic macrophages are removed inefficiently, culminating in the formation of necrotic areas or cores. Not surprisingly, enhancing macrophage-emigration from atherosclerotic lesions has been shown to reduce atherosclerotic progression [36]. Alternatively, defective clearance (efferocytosis) of apoptotic macrophages promotes expansion of necrotic cores in advanced lesions [16]. In this study, we observed larger necrotic areas as well as higher numbers of apoptotic cells in *CD13*$^{-/-}$ lesions, consistent with our phenotype. Since *CD13* negatively regulates receptor-mediated endocytosis of selected ligands, we hypothesized that *CD13*$^{-/-}$ macrophages would internalize more oxLDL via various receptors and thus increase apoptosis. However, our *in vitro* analysis of oxLDL-treated macrophages clearly showed that *CD13*$^{+/+}$ and *CD13*$^{-/-}$ macrophages expressed equivalent amounts of the CD36 and Lox-1 receptors and endocytosed similar amounts of oxLDL, ruling out potential uptake-dependent mechanisms for our phenotype.

We found that overall levels of oxidative stressors were significantly higher in oxLDL-treated macrophages and that inhibition of oxLDL uptake completely abolished production of oxidative stressors, strongly suggesting that increased oxLDL-induced oxidative stress promotes higher levels of apoptosis in *CD13*$^{-/-}$ macrophages. Not surprisingly, ROS production in response to oxLDL has been well documented both in macrophages *in vitro* and in atherosclerotic plaques *in vivo* [29,37,38] and perturbation of the various pro- and antioxidant enzyme systems clearly impacts atheroprogression [39,40]. These responses are proposed to be due in part to oxLDL-dependent effects on components of the innate immune TLR4 pathway [41,42]. OxLDL treatment stimulates functionally-relevant increases in expression of both theTLR4 receptor and its downstream mediator TRIF, since blocking or knockdown of these molecules inhibits oxLDL-induced pro-inflammatory responses and foam cell formation [43]. We have previously reported that the knockout of or antibody blockage of CD13 in macrophages and dendritic cells skews PAMP and DAMP-induced TLR4 signaling toward the TRIF-dependent endosomal pathway, thereby stimulating iNOS transcription and generating deleteriously high levels of oxidative stressors *in vitro* and *in vivo* [6]. Similarly, in this study we see increased nitric oxide levels in *CD13*$^{-/-}$ macrophages in response to oxLDL, strongly suggesting that in the atherosclerotic plaque, *CD13* controls oxLDL-induced inflammation and holds nitric oxide production in check via its effects on TLR4/TRIF signaling. Consequently, cells lacking CD13 are hyper-sensitized to oxidative stress-inducing agents such as oxLDL resulting in increased nitric oxide and elevated levels of cell death. Thus, in the context of atherosclerosis, rather than promoting damaging inflammation, CD13 acts to protect the cells from toxic oxidative stress and is atheroprotective.

Pertinent to these observations, we also found that *CD13*$^{-/-}$

macrophages showed significantly higher levels of basal apoptosis, independent of oxLDL treatment, which were observed with other *CD13*$^{-/-}$ primary cell isolates and cell lines engineered to lack *CD13* (unpublished data). We have previously demonstrated that cross-linking-induced activation of CD13 induces FAK phosphorylation and conversely, inhibition of FAK activation reduces CD13-mediated monocyte adhesion [13]. Similarly, lack of CD13 in skeletal muscle satellite stem cells impairs FAK phosphorylation and adhesion to the stem cell niche, resulting in defective self-renewal and aberrant early differentiation [15]. Since FAK signaling is critical to suppressing anoikis [44,45], it is logical that the diminished FAK signaling in the absence of CD13 renders cells susceptible to anoikis, a hypothesis that is currently under investigation. However, we believe that the increase in apoptosis of oxLDL-treated *CD13*$^{-/-}$ cells is independent of anoikis to a certain degree. This assumption is based on the fact that the treatment of differentiating human monocytes with LDL has been shown to up-regulate cell-adhesion molecules (CD49c) and down-regulate anoikis in early stages of differentiation [46]. Additionally, oxLDL treatment of peritoneal macrophages causes spreading rather than reduced adhesion in macrophages [47]. Therefore, we believe that the increased basal apoptosis seen in *CD13*$^{-/-}$ cells is mediated by anoikis, while increased apoptosis seen with oxLDL treatment is due to increased oxidative stress.

Limitations of this study include exclusion of females in the *in vivo* experiments, relatively subtle phenotypes, lack of later time points for *in vivo* experiments, limiting the study to a single model of atherosclerosis and our use of global *CD13*$^{-/-}$ mice. Clearly, sex is a variable in atherosclerosis in humans where men develop disease at an earlier age than women. Testing both sexes would strengthen our studies [48], but the extremely small litter sizes typically seen in C57Bl/6 background necessitated our use of the majority of females for breeding. The subtle phenotypes observed in our *in vivo* analyses can be attributed to the fact that we designed our experiment to primarily evaluate differences in immune cell infiltration which are typically evident at relatively early time points in this model. However, our unexpected phenotype of increased necrosis develops over longer time periods, as it is not clearly evident until our latest 15 week time point. It is possible that delaying harvest until to 20–25 weeks or longer on high fat diet may further amplify the differences between *CD13*$^{+/+}$ and *CD13*$^{-/-}$ mice. Alternatively, since the mice are born and mature in the absence of *CD13*, it is possible that compensatory mechanisms are activated that reduce the impact of its effects long-term [49,50]. Using inducible, macrophage-specific knockout animals would address this issue. A second well-characterized model of atherosclerosis focuses on lesion formation in ApoE knockout mice on high fat diet. Unfortunately, the genes encoding *ApoE* and *CD13* are both located on chromosome 7 which may interfere with production of double knockouts, leading us to choose the *Ldlr* knockout model. Finally, while a macrophage-specific knockout would likely provide clearer results in our studies as this would eliminate confounding contributions from other cell types, it may be argued that global knockout animals more faithfully recapitulate germline mutations in humans, where alterations in gene function would be present in all organs.

In conclusion, we have extended the findings of our previous studies to show that in addition to its other immunomodulatory functions in the innate immune system, CD13 plays a broader role in maintaining homeostatic levels of nitric oxide to protect myeloid cells in the inflammatory response to various detrimental extracellular stressors.

Conflicts of interest

The authors declared they do not have anything to disclose regarding conflict of interest with respect to this manuscript.

Financial support

This work was supported by NHLBI grants P01HL070694 and HL127449 (LHS) and P01HL029582 (JDS).

Author contributions

CVD: planned and performed all the *in vitro* experiments as well as histological analysis of lesions. Analyzed data from *in vitro* and *in vivo* experiments. Wrote the manuscript.

FEP: planned and performed *in vivo* high fat diet experiments. Analyzed data from *in vivo* experiments.

JDS: planned and performed total cholesterol and triglycerides quantification assays. Analyzed the data from these experiments.

LHS: designed and planned the project. Analyzed all the data and wrote the manuscript.

MG: planned and performed the experiments. Analyzed the data and edited the manuscript.

Appendix A. Supplementary data

Supplementary data to this article can be found online at https://doi.org/10.1016/j.atherosclerosis.2019.06.901.

References

[1] D. Ye, Y. Zhao, R.B. Hildebrand, et al., The dynamics of macrophage infiltration into the arterial wall during atherosclerotic lesion development in low-density lipoprotein receptor knockout mice, Am. J. Pathol. 178 (1) (2011) 413–422.
[2] K.J. Moore, F.J. Sheedy, E.A. Fisher, Macrophages in atherosclerosis: a dynamic balance, Nat. Rev. Immunol. 13 (10) (2013) 709–721.
[3] V. Stoneman, D. Braganza, N. Figg, et al., Monocyte/macrophage suppression in CD11b diphtheria toxin receptor transgenic mice differentially affects atherogenesis and established plaques, Circ. Res. 100 (6) (2007) 884–893.
[4] K.S. Michelsen, M.H. Wong, P.K. Shah, et al., Lack of Toll-like receptor 4 or myeloid differentiation factor 88 reduces atherosclerosis and alters plaque phenotype in mice deficient in apolipoprotein E, Proc. Natl. Acad. Sci. U. S. A. 101 (29) (2004) 10679–10684.
[5] H. Liu, W.L. Cheng, X. Jiang, et al., Ablation of interferon regulatory factor 3 protects against atherosclerosis in apolipoprotein E-deficient mice, Hypertension 69 (3) (2017) 510–520.
[6] M. Ghosh, J. Subramani, M.M. Rahman, L.H. Shapiro, *CD13* restricts TLR4 endocytic signal transduction in inflammation, J. Immunol. 194 (9) (2015) 4466–4476.
[7] M. Ghosh, B. McAuliffe, J. Subramani, S. Basu, L.H. Shapiro, *CD13* regulates dendritic cell cross-presentation and T cell responses by inhibiting receptor-mediated antigen uptake, J. Immunol. 188 (11) (2012) 5489–5499.
[8] S.V. Bhagwat, J. Lahdenranta, R. Giordano, W. Arap, R. Pasqualini, L.H. Shapiro, *CD13*/APN is activated by angiogenic signals and is essential for capillary tube formation, Blood 97 (3) (2001) 652–659.
[9] P. Mina-Osorio, B. Winnicka, C. O'Conor, et al., *CD13* is a novel mediator of monocytic/endothelial cell adhesion, J. Leukoc. Biol. 84 (2) (2008) 448–459.
[10] F.E. Pereira, C. Cronin, M. Ghosh, et al., *CD13* is essential for inflammatory trafficking and infarct healing following permanent coronary artery occlusion in mice, Cardiovasc. Res. 100 (1) (2013) 74–83.
[11] B. Winnicka, C. O'Conor, W. Schacke, et al., *CD13* is dispensable for normal hematopoiesis and myeloid cell functions in the mouse, J. Leukoc. Biol. 88 (2) (2010) 347–359.
[12] J. Schindelin, I. Arganda-Carreras, E. Frise, et al., Fiji: an open-source platform for biological-image analysis, Nat. Methods 9 (7) (2012) 676–682.
[13] J. Subramani, M. Ghosh, M.M. Rahman, et al., Tyrosine phosphorylation of *CD13* regulates inflammatory cell-cell adhesion and monocyte trafficking, J. Immunol. 191 (7) (2013) 3905–3912.
[14] M. Busch, T.C. Westhofen, M. Koch, M.B. Lutz, A. Zernecke, Dendritic cell subset distributions in the aorta in healthy and atherosclerotic mice, PLoS One 9 (2) (2014) e88452.
[15] M.M. Rahman, M. Ghosh, J. Subramani, G.H. Fong, M.E. Carlson, L.H. Shapiro, *CD13* regulates anchorage and differentiation of the skeletal muscle satellite stem cell population in ischemic injury, Stem Cell. 32 (6) (2014) 1564–1577.
[16] E. Thorp, D. Cui, D.M. Schrijvers, G. Kuriakose, I. Tabas, Mertk receptor mutation reduces efferocytosis efficiency and promotes apoptotic cell accumulation and plaque necrosis in atherosclerotic lesions of apoe-/- mice, Arterioscler. Thromb. Vasc. Biol. 28 (8) (2008) 1421–1428.
[17] R. Kato, C. Mori, K. Kitazato, et al., Transient increase in plasma oxidized LDL during the progression of atherosclerosis in apolipoprotein E knockout mice, Arterioscler. Thromb. Vasc. Biol. 29 (1) (2009) 33–39.
[18] V.V. Kunjathoor, M. Febbraio, E.A. Podrez, et al., Scavenger receptors class A-I/II and CD36 are the principal receptors responsible for the uptake of modified low

density lipoprotein leading to lipid loading in macrophages, J. Biol. Chem. 277 (51) (2002) 49982–49988.
[19] A. Boullier, Y. Li, O. Quehenberger, et al., Minimally oxidized LDL offsets the apoptotic effects of extensively oxidized LDL and free cholesterol in macrophages, Arterioscler. Thromb. Vasc. Biol. 26 (5) (2006) 1169–1176.
[20] E.S. Wintergerst, J. Jelk, C. Rahner, R. Asmis, Apoptosis induced by oxidized low density lipoprotein in human monocyte-derived macrophages involves CD36 and activation of caspase-3, Eur. J. Biochem. 267 (19) (2000) 6050–6059.
[21] E. Brauchle, S. Thude, S.Y. Brucker, K. Schenke-Layland, Cell death stages in single apoptotic and necrotic cells monitored by Raman microspectroscopy, Sci. Rep. 4 (2014) 4698.
[22] Q. Shao, F. Han, S. Peng, B. He, Nur77 inhibits oxLDL induced apoptosis of macrophages via the p38 MAPK signaling pathway, Biochem. Biophys. Res. Commun. 471 (4) (2016) 633–638.
[23] J.E. Murphy, R.S. Vohra, S. Dunn, et al., Oxidised LDL internalisation by the LOX-1 scavenger receptor is dependent on a novel cytoplasmic motif and is regulated by dynamin-2, J. Cell Sci. 121 (Pt 13) (2008) 2136–2147.
[24] A. Yurdagul Jr., F.J. Sulzmaier, X.L. Chen, C.B. Pattillo, D.D. Schlaepfer, A.W. Orr, Oxidized LDL induces FAK-dependent RSK signaling to drive NF-kappaB activation and VCAM-1 expression, J. Cell Sci. 129 (8) (2016) 1580–1591.
[25] C.C. Hsieh, M.H. Yen, C.H. Yen, Y.T. Lau, Oxidized low density lipoprotein induces apoptosis via generation of reactive oxygen species in vascular smooth muscle cells, Cardiovasc. Res. 49 (1) (2001) 135–145.
[26] A. Negre-Salvayre, N. Auge, C. Duval, et al., Detection of intracellular reactive oxygen species in cultured cells using fluorescent probes, Methods Enzymol. 352 (2002) 62–71.
[27] K. Yang, X. Wang, Z. Liu, et al., Oxidized low-density lipoprotein promotes macrophage lipid accumulation via the toll-like receptor 4-Src pathway, Circ. J. 79 (11) (2015) 2509–2516.
[28] L. Chavez-Sanchez, M.G. Garza-Reyes, J.E. Espinosa-Luna, K. Chavez-Rueda, M.V. Legorreta-Haquet, F. Blanco-Favela, The role of TLR2, TLR4 and CD36 in macrophage activation and foam cell formation in response to oxLDL in humans, Hum. Immunol. 75 (4) (2014) 322–329.
[29] Y. Wang, G.Z. Wang, P.S. Rabinovitch, I. Tabas, Macrophage mitochondrial oxidative stress promotes atherosclerosis and nuclear factor-kappaB-mediated inflammation in macrophages, Circ. Res. 114 (3) (2014) 421–433.
[30] J. Blanc, M.C. Alves-Guerra, B. Esposito, et al., Protective role of uncoupling protein 2 in atherosclerosis, Circulation 107 (3) (2003) 388–390.
[31] S.W. Ballinger, C. Patterson, C.A. Knight-Lozano, et al., Mitochondrial integrity and function in atherogenesis, Circulation 106 (5) (2002) 544–549.
[32] K.M. Robinson, M.S. Janes, J.S. Beckman, The selective detection of mitochondrial superoxide by live cell imaging, Nat. Protoc. 3 (6) (2008) 941–947.
[33] M. Ghosh, C. Gerber, M.M. Rahman, et al., Molecular mechanisms regulating *CD13*-mediated adhesion, Immunology 142 (4) (2014) 636–647.
[34] G.H. Fong, Potential contributions of intimal and plaque hypoxia to atherosclerosis, Curr. Atheroscler. Rep. 17 (6) (2015) 510.
[35] J. Llodra, V. Angeli, J. Liu, E. Trogan, E.A. Fisher, G.J. Randolph, Emigration of monocyte-derived cells from atherosclerotic lesions characterizes regressive, but not progressive, plaques, Proc. Natl. Acad. Sci. U. S. A. 101 (32) (2004) 11779–11784.
[36] J.M. van Gils, M.C. Derby, L.R. Fernandes, et al., The neuroimmune guidance cue netrin-1 promotes atherosclerosis by inhibiting the emigration of macrophages from plaques, Nat. Immunol. 13 (2) (2012) 136–143.
[37] W. Liu, Y. Yin, Z. Zhou, M. He, Y. Dai, OxLDL-induced IL-1 beta secretion promoting foam cells formation was mainly via CD36 mediated ROS production leading to NLRP3 inflammasome activation, Inflamm. Res. 63 (1) (2014) 33–43.
[38] Park JG, Oh GT. The Role of Peroxidases in the Pathogenesis of Atherosclerosis. (1976-670X (Electronic)).
[39] P.A. Detmers, M. Hernandez, J. Mudgett, et al., Deficiency in inducible nitric oxide synthase results in reduced atherosclerosis in apolipoprotein E-deficient mice, J. Immunol. 165 (6) (2000) 3430–3435.
[40] H. Li, S. Horke, U. Forstermann, Vascular oxidative stress, nitric oxide and atherosclerosis, Atherosclerosis 237 (1) (2014) 208–219.
[41] M. Chen, W. Li, Y. Zhang, J. Yang, MicroRNA-20a protects human aortic endothelial cells from Ox-LDL-induced inflammation through targeting TLR4 and TXNIP signaling, Biomed. Pharmacother. 103 (2018) 191–197.
[42] J. Guo, W. Liang, J. Li, J. Long, Knockdown of FSTL1 inhibits oxLDL-induced inflammation responses through the TLR4/MyD88/NF-kappaB and MAPK pathway, Biochem. Biophys. Res. Commun. 478 (4) (2016) 1528–1533.
[43] Y. Wu, J. Ye, R. Guo, X. Liang, L. Yang, TRIF regulates BIC/miR-155 via the ERK signaling pathway to control the ox-LDL-induced macrophage inflammatory response, J Immunol Res (2018) 6249085 2018.
[44] J. Alanko, A. Mai, G. Jacquemet, et al., Integrin endosomal signalling suppresses anoikis, Nat. Cell Biol. 17 (11) (2015) 1412–1421.
[45] S.M. Frisch, K. Vuori, E. Ruoslahti, P.Y. Chan-Hui, Control of adhesion-dependent cell survival by focal adhesion kinase, J. Cell Biol. 134 (3) (1996) 793–799.
[46] R. Escate, T. Padro, L. Badimon, LDL accelerates monocyte to macrophage differentiation: effects on adhesion and anoikis, Atherosclerosis 246 (2016) 177–186.
[47] Y.I. Miller, S. Viriyakosol, C.J. Binder, J.R. Feramisco, T.N. Kirkland, J.L. Witztum, Minimally modified LDL binds to CD14, induces macrophage spreading via TLR4/MD-2, and inhibits phagocytosis of apoptotic cells, J. Biol. Chem. 278 (3) (2003) 1561–1568.
[48] P. Robinet, D.M. Milewicz, L.A. Cassis, N.J. Leeper, H.S. Lu, J.D. Smith, Consideration of sex differences in design and reporting of experimental arterial pathology studies-statement from ATVB council, Arterioscler. Thromb. Vasc. Biol. 38 (2) (2018) 292–303.
[49] B. To, E.R. Andrechek, Transcription factor compensation during mammary gland development in E2F knockout mice, PLoS One 13 (4) (2018) e0194937.
[50] S. Kim, R.F. Titcombe, H. Zhang, et al., Network compensation of cyclic GMP-dependent protein kinase II knockout in the hippocampus by Ca2 + -permeable AMPA receptors, Proc. Natl. Acad. Sci. U. S. A. 112 (10) (2015) 3122–3127.